IRANIAN SOCIETY of CRYSTALLOGRAPHY and MINERALOGY

Vol. 16, No. 4, Winter 1387/2009

IRANIAN JOURNAL of CRYSTALLOGRAPHY and MINERALOGY

Influence of N_2- and Ar-ambient annealing on the physical properties of SnO_2: Co transparent conducting films prepared by spray pyrolysis technique

A. Gholizadeh, N. Tajabor, M. R. Alinejad

Department of Physics, Ferdowsi University of Mashhad, Mashhad, Iran
Email: ah_gh1359@yahoo.com

(Received: 8/4/2008, in revised form: 18/12/2008)

Abstract: In this contribution, the Co doped SnO_2 transparent semi-conducting films are prepared by spray pyrolysis technique and the influence of N_2-and Ar-ambient annealing on their structural, electrical and optical properties are studied. The SnO_2:Co thin films were deposited on the glass substrate at substrate temperature of 480 ˚C using an aqueous-ethanol solution consisting of tin and cobalt chloride. Doping levels of cobalt chloride have been changed from 0 to 14 wt. % in solution. Analysis of the X-ray diffraction patterns show that 'a' and 'V' parameters of the tetragonal unit cell decrease with increasing impurity content, while c parameter pass through a minimum for a acceptor dopant concentration of 8 wt. % or [Co]/[Sn] atomic ratio equal to 20 atm.% in solution. The N_2-and Ar-ambient annealing causes increase of the electrical resistivity, band gap energies, and transparency of the cobalt doped samples.

Keywords: *Transparent Oonducting Oxides* (TCOs)*; Dilute Magnetic Semiconductors (*DMSs*); Spray Pyrolysis.*

1. Introduction

The TCOs exhibit high optical transparency and good electrical conductivity so that they have received many attentions in both industry and research activities [1, 2]. Nowadays, modern information technology in new nano-electronic and photonic devices utilizes the spin degree of freedom in the magnetic TCOs. Towards this end; one approach is to introduce small amounts of the magnetic dopants (such as Co, Mn, Fe and Ni) into nonmagnetic solids [3-7]. These families of TCOs that are called dilute magnetic semiconductors (DMSs) have been examined for SnO_2, In_2O_3, TiO_2 and ZnO transparent thin films [8-12].

SnO_2 is a wide-band gap semiconductor with baud-gap of E_g = 3.6 ~ 4.2 eV. In addition to the excellent optical transparency and high Curie temperature (T_c), SnO_2 is very stable chemically [1, 13]. It is known that the electrical resistivity of thin films of SnO_2 depends on the concentration of oxygen vacancies within their rutile crystal structure (S.G. P4/nmm) [14]. During last decade, many attentions had been paid to tune oxygen vacancies by doping various metallic elements, changing deposition technique and annealing at certain atmospheres [15-19]. Previous results show that substitution of a few percent of Sn^{+4} ions by Co^{+2} not only affects concentration of oxygen vacancies and charge carriers [20], but also introduces cobalt doped SnO_2 films which are DMSs with high Curie temperature (T_c = 650 °K) and giant magnetic moment per Co- atoms which has not been seen in any DMS system, thus far [21]. So, SnO_2: Co films are potentially interesting DMSs for using in new spintronic and magnetooptic devices.

In this work Co-doped SnO_2 films with various doping levels have been deposited using spray pyrolysis technique. Then, structural, electrical,

and optical properties of the prepared samples have been studied. In the study of SnO_2 crystallites, the (110), (101) and (100) are recognized as three significant crystallographic planes. Previous theoretical and experimental results indicate that the (110) plane has lowest surface energy and so stability [22]. Surface energy, which is the characteristic parameter of the faceting behavior of SnO_2 polycrystalls, depends on the chemical potential of oxygen and deviation from the surface stoichiometry. Considering that the chemical stoichiometry of planes is affected by the deposition method and post annealing of the deposited films at certain atmospheres, we expect that the faceting behavior of the Co-doped SnO_2 samples may be controlled by changing these parameters. Therefore, the effects of N_2- and Ar-ambient annealing on the faceting, electrical and optical properties of Co-doped SnO_2 films are studied.

2. Experimental

2.1 Material preparation and deposition of films

The undoped SnO_2 thin films were deposited using an aqueous-ethanol solution including $SnCl_2.2H_2O$, H_2O and CH_3CH_2OH with the same weight percentage (1: 1: 1) and a few ml of hydrochloric acid by the spray pyrolysis technique. Also, Co doped SnO_2 films have been prepared using 0, 2, 4, 8, 10, 12, 14 wt. % of $CoCl_2.6H_2O$ that added to the initial solution without any changes in the clarity of the solution. The spray solution compositions and atomic concentration ratios in the prepared solutions are given in Table 1.

For film deposition, a clean substrate (the glass substrates with 1 mm thickness and 25 × 75 mm dimensions), was placed on the hot plate at temperatures ranging from 480-500°C, which is known to be the optimal range for the formation of SnO_2 films [23]. Then solution was sprayed at the following conditions: carrier-gas pressure (O_2): 1.7-2 atm., flow rate of solution: 14 ml/min, solution volume: 10 cc and substrate-to-nozzle distance: 45 cm. For preventing reduction at hot plate temperature, spraying was done in short time intervals. All samples were prepared almost with the same conditions. The metallic salt solution, when sprayed onto a hot substrate, pyrolitically decomposes and a chemical reaction takes place on the heated substrate and at least a thin layer of SnO_2 (undoped or doped) is deposited. Thin films with about 0.4 μm thickness are prepared in this manner, as estimated by SEM micrographs and optical method. After deposition, the original thin samples were cut into 13 × 26 mm dimensions and four similar series of the Co-doped SnO_2 films were prepared for executing post-annealing treatments. Below, we will call each one of these series in the following manner. SnO_2: Co transparent conducting films prepared with different Co concentrations: (Series 1) as-deposited and (Series 2) annealed at 550°C in the Ar, and, (Series 3) in the N_2 atmospheres for 5h, and, (Series 4) in Ar followed by N_2 for 5h, respectively.

Table 1. Composition of the Co-doped SnO_2 solutions.

$Co\ Cl_2.6H_2O$ (wt %. in solution)	*$SnCl_2.2H_2O$ (M)*	*$CoCl_2.6H_2O$ (M)*	*[Co] / [Sn] (atm.% in solution)*
0	14.6	0	0
2	14.6	0.73	5
4	14.6	1.46	10
8	14.6	2.92	20
10	14.6	3.65	25
12	14.6	4.30	30
14	14.6	5.11	35

2.2 Structural

Microstructure of the samples was analyzed using polarized optical microscope as well as scanning electron microscope. Frequency distribution of the grains size within the samples has been studied using LICA analyzer (QW500 model) based on the optical images. The X-ray diffraction patterns of the prepared thin films were taken by a D8 Advance Bruker system using Cu-Kα radiation. Phase analysis of the samples has been done based on the XRD patterns. The information on microstrain (ε_s) and the crystallite size (D) of the deposited films have been obtained from the full-width at half-maximum (FWHM) of the diffraction peaks (β) via Williamson-Hall relation [24]:

$$\frac{\beta\cos\theta}{\lambda}=\frac{1}{D}+\frac{\varepsilon_s\sin\theta}{\lambda} \quad (1)$$

And sherrer' s relation:

$$D=\frac{0.9\,\lambda}{\beta\cos\theta} \quad (2)$$

Lattice parameter refinements are performed using CELREF software from LMGP institute (Grenoble - France).

2.3 Electrical

Electrical measurements consist of the resistivity; carrier concentration and mobility determination have been done via Van der Pauw method [25]. In addition, Seebeck's effect measurements were performed for distinction of the carrier type.

2.4 Optical

Absorption coefficient is suitable tool for studying band gap energy. Optical transmission and absorption spectra of the Co-doped SnO_2 films between 200 and 1000 nm wave lengths have been recorded at room temperature using HP-UV-Vis system (Agilent 8453, model). For estimating band gap, the optical absorption coefficient (α(λ)) was calculated from the absorption spectra (A(λ)) using the following equation [26]:

$$\alpha(\lambda)=2.303\,\frac{A(\lambda)}{t} \quad (3)$$

In which, t is thickness of the deposited film. Then, a self consistence rote based on the following relation was used for deducing optical band gap energy, E_g:

$$(\alpha h\nu) = B(h\nu - E_g)^r \quad (4)$$

Where, B is an energy-independent constant and r is a parameter refers to the type of excitation of carriers across the band gap. In fact, r = 0.5, 2, 1.5 and 3 corresponds to the direct, indirect, forbidden direct and forbidden indirect type of transitions, respectively. Details of this method can be found in ref. [27].

For estimating Urbach edge (E_0), we refer to the following relation that is valid for direct optical transitions in the spectral range [28],

$$\alpha(h\nu)=\alpha_o\exp\left(\frac{h\nu-E_g}{E_o}\right) \quad (5)$$

Where, α_o is the optical absorption coefficient at the band gap energy edge. The value of E_o can be deduced as inverse of the slope of $\ln(\alpha)$ vs. $h\nu$ plot.

Thickness of the deposited films has been estimated using following formula:

$$t=\frac{1}{2\left(\frac{1}{\lambda_1}-\frac{1}{\lambda_2}\right)n_o} \quad (6)$$

In which, λ_1 and λ_2 are wavelengths of two consecutive maximums in the transmission spectra. Also, n_o is the refraction index of the films which has been selected equal to 2 based on the reported values for the mean value of the refraction index of TCOs [29].

3. Results and discussion

Typical optical micrographs of the samples are shown in Fig. 1. These micrographs consist of a uniform bright background and a mixture of dark and white regions (grains). Similarly, SEM micrographs confirm same microstructure (Fig. 2a). Local EDX compositional analysis shows that these dark grains mainly contain O, Sn and Co atoms, while the white grains only consist of O and Sn atoms (Fig. 2b and c). As shown in Fig. 1, one may find very small ~1 to 25 μm size of dark grains in all four images, except in Fig. 1a.

The XRD patterns of the samples are shown in Fig. 3. It is clear that as-deposited layers are fine polycrystalline and some Co-doped films are self-orientated. Comparison of the sharpness of diffraction peaks of the undoped films indicate that the size of crystallites considerably increases by annealing at N_2-ambient, while Ar-ambient has not such an effect. The preferential orientation and faceting behaviors can be observed in Fig. 4, where the normalized intensity of the (110), (101), (200) and (211) Brag's peaks are plotted as a function of cobalt content for the series 1 samples.

Comparative analysis of the XRD patterns indicates that the faceting characteristics are conserved after post annealing treatments. It is clear that the ratio of the intensity of (200) diffraction peaks considerably increases with increasing concentration of Co impurities to 25 atm.%. Analyses of these results show the faceting of films along tetragonal a-axis, especially for the samples with 20 and 25 atm.% impurity level. The preferential alignment usually originates from the created strains during deposition of films that are a function of deposition parameters such as substrate temperature and deposition rate [30]. Here, the observed faceting can be attributed to the decrease of the surface energy density of the (200) plane with respect to that of (110) after partial substitution of Sn by Co [22].

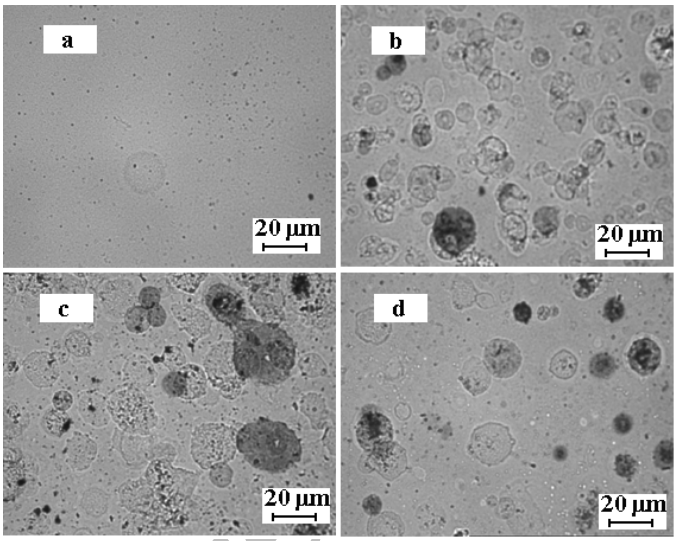

Fig. 1. Polarized optical micrographs of Co-doped SnO_2 thin films: (a) 0; (b) 10; (c) 20; and (d) 30 atm.%.

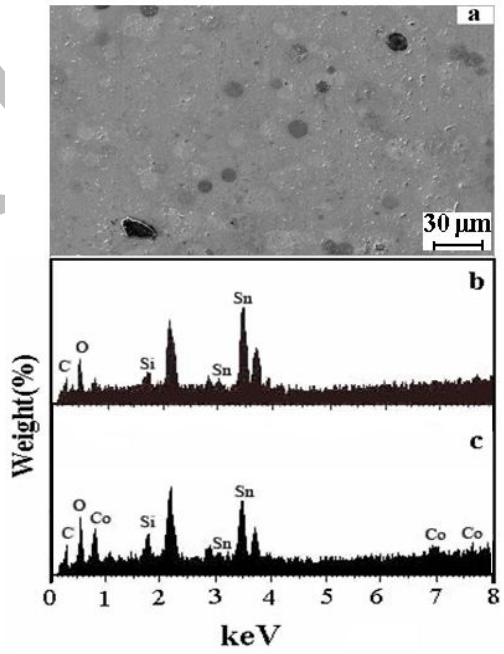

Fig. 2. (a) A typical SEM micrograph of the 20 atm.% Co-content in solution. (b) And (c) Local EDX analysis of the elemental composition of the white and dark grains, respectively.

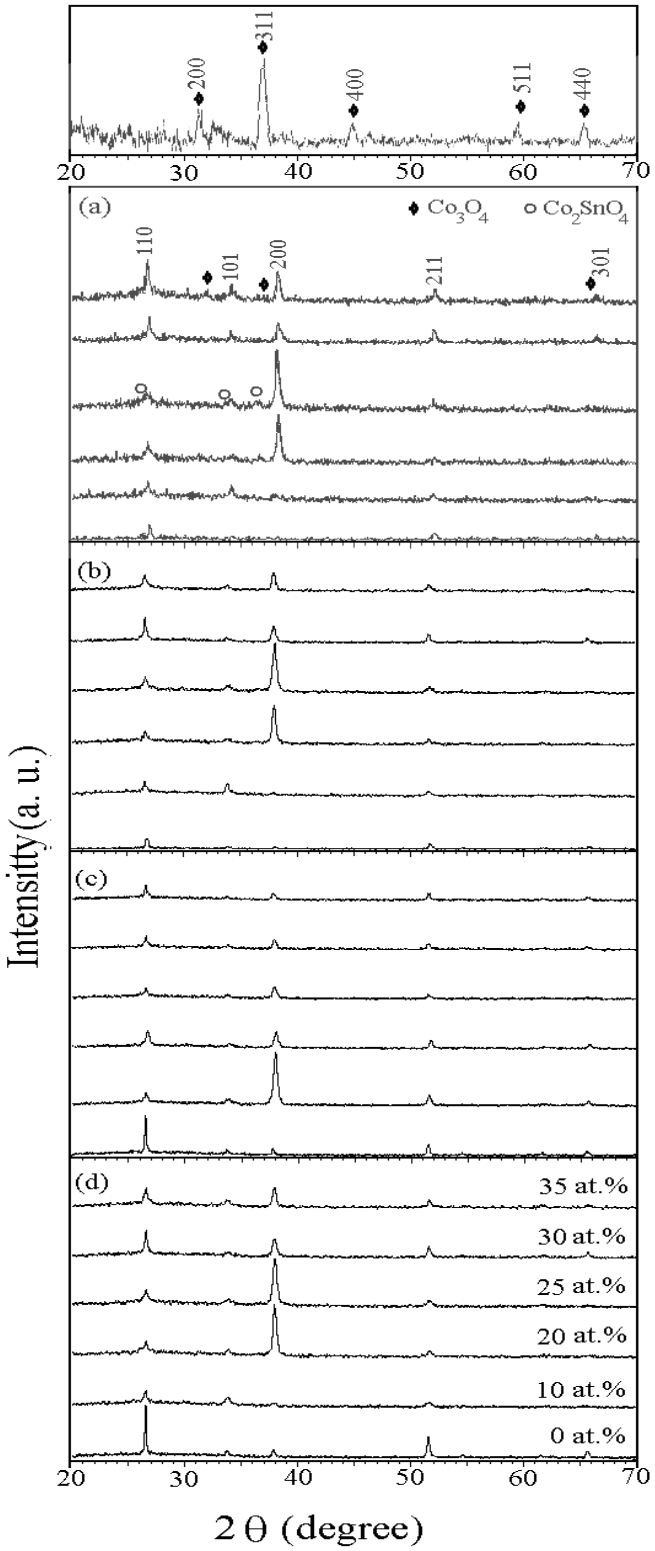

Fig. 3. XRD patterns of SnO_2:Co transparent conducting films prepared with different Co concentration: (a) as-deposited, (b) annealed at 550°C in Ar, (c) in N_2 atmospheres for 5h, and, (d) in Ar followed by N_2 for 5h. The XRD pattern of Co_3O_4 is given on the top of figure, too.

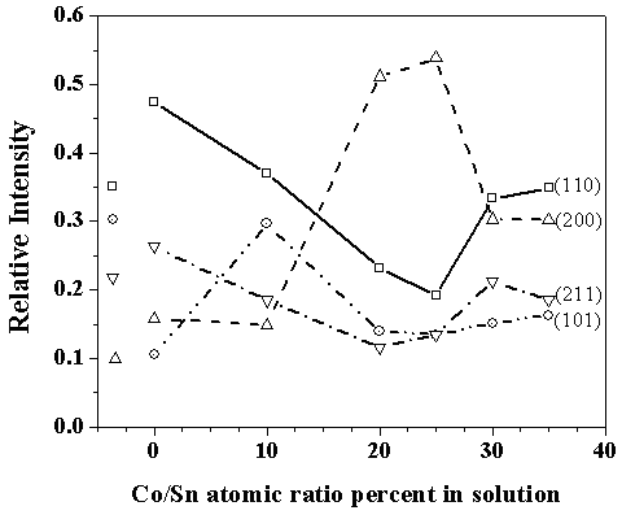

Fig. 4. Normalized intensity of the (110), (101), (200) and (211) Brag's peaks of the series 1 samples vs. Co/Sn atomic ratio. Normalized intensities were deduced by dividing intensity of each peak to the sum of intensities of all the 4 peaks. Also, normalized intensities in the standard pattern of SnO_2 powder have been given in the left hand side of the figure by appropriate symbols.

As shown in Fig. 3, some additional peaks appear in the XRD pattern of series 1 sample with more than 20 atm.% doping level. These additional peaks correspond to the standard diffraction pattern of Co_2SnO_4 and Co_3O_4 phases with cubic structure. The presence of such phases also reported in $Zn_{1-x}Co_xO$ samples [31] and $Sn_{1-x}Co_xO_2$ [32] samples, which may affect structural, electrical and optical properties of the studied samples. The unwanted phases considerably decrease after annealing and all the annealed samples seem to be single phase.
The derived rutile lattice parameters of the series 1 samples are given in Fig. 5. This figure shows that 'a' and 'V' (Volume of unit cell) parameters of the tetragonal unit cell decrease with increasing cobalt content, while 'c' parameter passes through a minimum for 20 atm % doping level. Calculated lattice parameters of the annealed samples exhibit similar behavior, too. It is well known that the ionic radius of Co^{+3} (0.63 Å) is less, while the ionic radius of Co^{+2} (0.72 Å) is grater than that of Sn^{+4} (0.71 Å) [33]. Therefore, decrease of 'a' and 'V' is natural consequence of the substitution of Co^{+3} ions instead of Sn^{+4} in the SnO_2 rutile structure.

In addition, observed enhancements of the full width at half the maximum (FWHM) of the XRD peaks by increasing Co-content, indicating possible changes in the crystallite size and microstrains. The crystallite sizes and microstrains have been calculated based on the (110), (200) and (101) Brag's peaks in the XRD patterns (Fig. 6). These results show that the size of crystallite decreases with increasing microstrain (and conversely), and both of them become extermum about 20 atm.% doping level. In fact, minimum of the 'c' parameter is accompanied by the minimum size of crystallites and the maximum value of microstrains. So, one may attribute the abnormal minimum of the 'c' lattice parameter to the increase of the introduced stress after substitution of Sn by Co in the rutile structure. Also, decrease of the microstrains for more than 20 atm.% doping level is compensated by the formation of Co_2SnO_4 and Co_3O_4 unwanted phases in the series 1 samples.

Results of the electrical measurements exhibit gradual increase of the resistivity with cobalt additives (Table 2). Also, the carrier concentration decreases by increasing Co content to 10 atm.%, and then, approximately remains constant for additional doping level. Decrease of the n-type carrier concentration can be attributed to the substitution of Sn^{+4} by smaller Co^{+3} in the rutile unit cell. Although, by this trend one may expect that the type of carriers should gradually changes from n^- to p^+ with increasing doping level, but results of the Seebeck's measurements emphasize on the n-type carriers in all studied samples. This can be explained considering that the XRD patterns show the complete penetration of Co atoms within crystal structure of SnO_2 only for

lower than 25 atm.% doping levels. Variation of the mobility in terms of carrier concentration is due to a combination of ionized impurity and grain boundary scattering mechanisms where the former seems to be dominated [34].

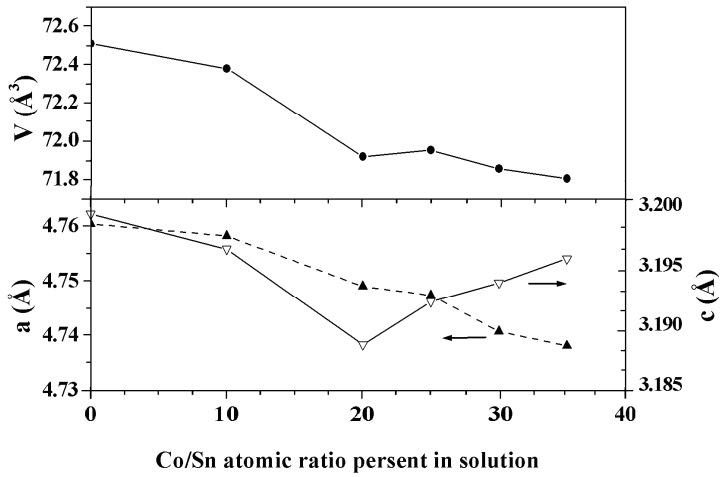

Fig. 5. Variation of the crystal lattice parameters of the series 1 samples vs. Co/Sn atomic ratio.

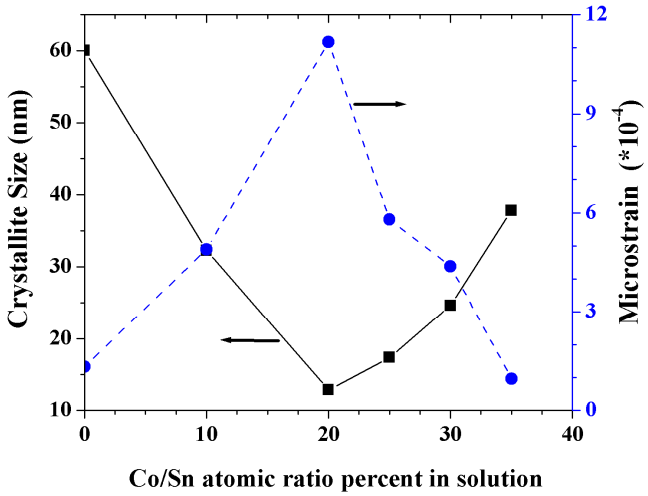

Fig. 6. Crystallite sizes and microstrains calculated based on the (110), (200) and (101) Brag's peaks in the XRD patterns of the series 1 samples vs. Co/Sn atomic ratio.

Table 2. Resistivity (ρ), carrier concentration (n) and Seebeck's coefficient (α) of the series 1 samples.

Sample (atm.%)	*Thickness (nm)*	*ρ (Ω . cm)*	*$n*10^{16}$ (cm^{-3})*	*α (μV/K)*
0	~ 400	0.025	-766.00	-140
5	~ 400	2.32	-1.27	-75
10	~ 400	4.23	-0.77	-60
20	~ 400	2.92	-0.89	-40
25	~ 400	16.50	-0.69	-50
30	~ 400	25.00	-0.67	-55
35	~ 400	28.10	-0.64	-65

Results of the electrical measurements after annealing are shown in Fig. 7. It is clear that the annealing cause increase of the electrical resistivity of the cobalt doped samples and this increase is mostly a function of the annealing duration. In addition, comparison of the effect of N_2-ambient and Ar-ambient annealing on the resistivity indicates that about 40 % of this increase should be due to penetration of the nitrogen ions within the rutile structure. The structural and compositional relaxations should be origin of the remained 60 % of the increase of resistivity.

Optical spectra show that transparency of the samples in the visible region decreases between 10 and 40 % by increasing Co-content (Figs. 8, 9). This was expected because of increase of the average size of dark grains of Co content as depicted in fig. 3. Films thickness was estimated 400 nm by using eq. (6). However, transparency of the samples with lower that 30 atm.% doping levels are slightly increased after post annealing treatments. The observed increase may be ascribed to the decrease of the surface defects due to post annealing treatments [35].

Corresponding best-fitted values of the band gap energy that are deduced via the self-consistence rote of eq. (4) are given in Table 3, where the value of r is consistently supposed to be 0.5 for all samples which indicate mechanism of the excitations is based on the direct transitions in all samples. Also, for showing relationship of the band gap energy variations and the Urbach energy, these two quantities are drawn versus Co-doping level in Fig. 10. Analogous variations of the Urbach and the band gap energies in this figure indicate that the observed changes in the band gap can be due to the effect of Co on the crystalline perfection of SnO_2.

The derived bang gap energies are shown in Fig. 11, which in all samples become minimized at about 10 atm.% doping level. However, these are some increase in them by post annealing treatment.

4. Conclusions

The Co doped SnO_2 TCOs are prepared by spray pyrolysis technique and the influence of N_2-and Ar-ambient annealing on their structural, electrical and optical properties were studied. The XRD patterns show that some of the Co-doped films exhibit a faceting characteristic that is conserved after post annealing treatments. This faceting is attributed to the decrease of the surface energy density of the (200) plane respect to that of (110) after substitution of Sn by Co.

Analyses of the XRD patterns show that the size of crystallite decreases with increasing microstrain and both of them become extermum at about 20 atm.% doping level. In addition, 'a' and 'V' parameters of the tetragonal unit cell decrease with increasing impurity content, while c parameter pass through a minimum at 20 atm.% impurity level.

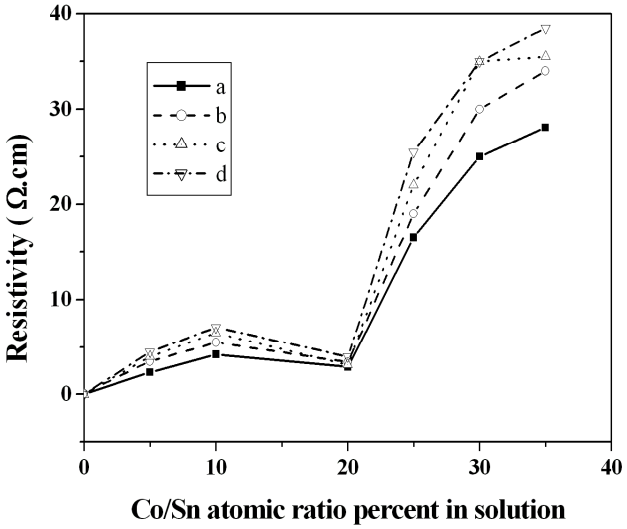

Fig. 7. Electrical resistivity of SnO_2:Co transparent conducting films prepared with different Co concentration (a) as-deposited, (b) annealed at 550°C in Ar, (c) in N_2 atmospheres for 5h, and, (d) in Ar followed by N_2 for 5h.

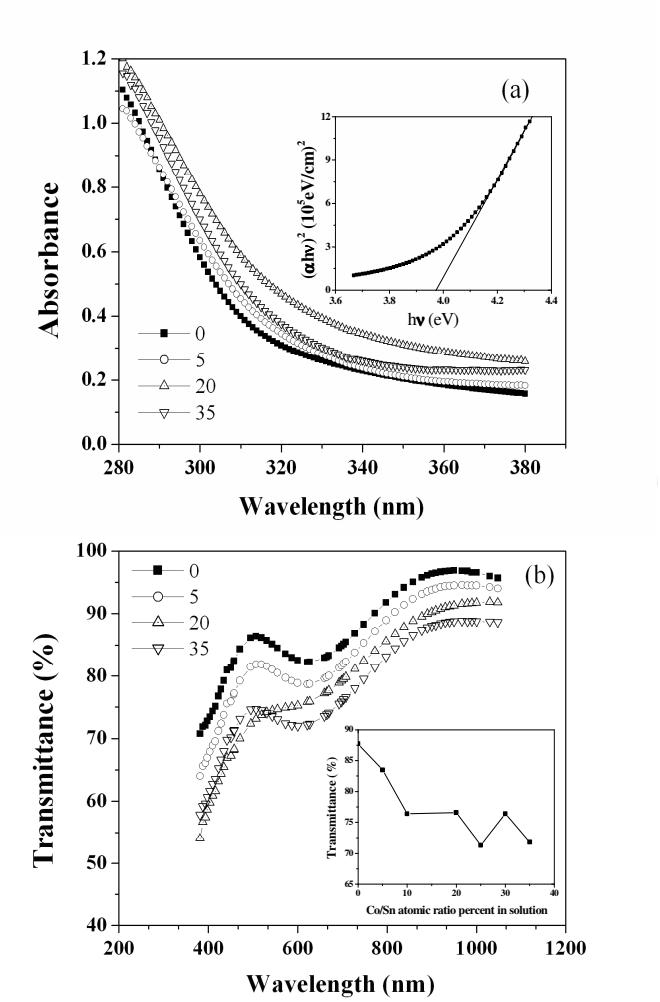

Fig. 8. Typical (a) absorbance and (b) transparency spectra of the series 1 samples vs. wavelength for 0, 5, 20, and 35% of Co/Sn atomic ratio. In the inset of fig.(a), $(\alpha h\nu)^2$ vs. hν for 10% of Co/Sn atomic ratio, from which the optical band gap value is deduced. In the inset of fig.(b), variation of the transmittance of SnO2: Co transparent conducting films at typical 600 nm wavelength.

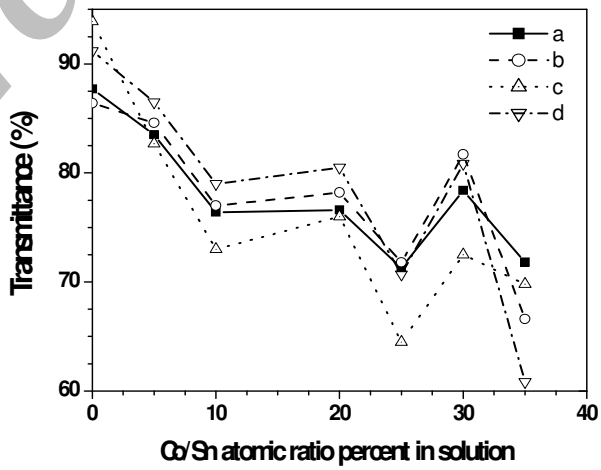

Fig. 9. The optical transmittance of SnO_2: Co transparent conducting films prepared with different Co concentration: (a) as-deposited, (b) annealed at 550°C in Ar, (c) in N_2 atmospheres for 5h, and, (d) in Ar followed by N_2 for 5h.

Table 3. Band gap energy, Urbach energy and B constant (as defined in eq. 4) of the series 1 samples.

Sample (atm.%)	E_g *(ev)*	E_0 *(mev)*	B $(cm^{-2}.ev)^{1/2}$
0	4.053	387	741015
5	3.995	406	661180
10	3.950	531	606495
20	3.960	480	625415
25	3.970	470	687380
30	3.986	450	736540
35	4.010	390	747460

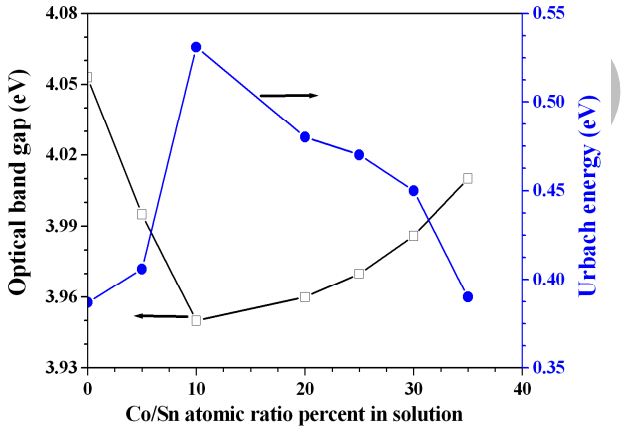

Fig. 10. Variations of the Urbach (E_0) and the band gap energy (E_g) of the series 1 samples vs. Co/Sn atomic ratio

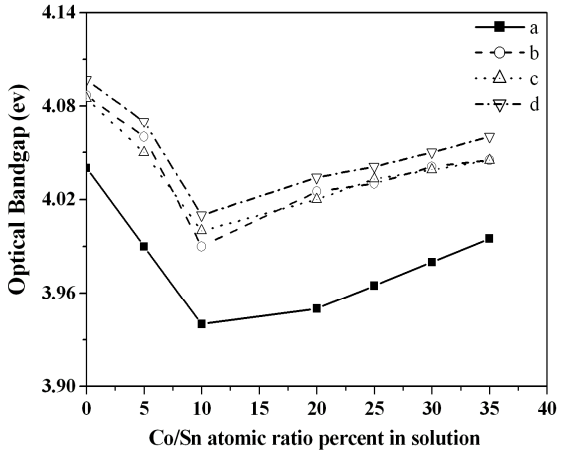

Fig. 11. Variations of the band gap energy of SnO_2: Co transparent conducting films prepared with different Co concentration (a) as-deposited, (b) annealed at 550°C in Ar, (c) in N_2 atmospheres for 5h, and, (d) in Ar followed by N_2 for 5h.

Electrical measurements demonstrate gradual increase of the resistivity by increasing doping level. The annealing causes increase of the electrical resistivity of the cobalt doped samples and this increase is mostly a function of the annealing duration. About 40 % of this increase should be due to penetration of the nitrogen ions within the rutile structure and the remained 60 % may be attributed to the structural and compositional relaxations.

The optical spectra show that the transparency of the samples in the visible region decreases between 10 and 40 % by increasing cobalt content. However, the transparency of the samples with

lowers than 30 atm.% doping level slightly increases after post annealing treatments.

The bang gap energies become minimized at about 10 atm.% doping level while these are some increase by post annealing treatment. In addition, the mechanism of excitations is based on the direct transitions in all samples. The observed band gap variations may attribute to the defect concentration and crystalline perfection.

References

[1] Brian G. Lewis and David C. Paine, *"MRS Bulletin"*, August (2000) pp. 22-27.
[2] Roy G. Gordon, *"MRS Bulletin"*, August (2000) pp. 52-57.
[3] T. Dietl, *"Nature Materials",* 2 (2003) 646.
[4] W. Prellier, A. Fouchet, B Mercey, J. Phys.: Condens Matter 15 (2003) R1583; Ref. 54, 55 therein.
[5] F. Matsukura, H. Ohno, T. Dietl, *"III-V Ferromagnetic Semiconductors, Handbook of magnetic materials"*, ed. by K. H. J. Busschow, Elsevier Science, Vol. 14, Chapter 1 (2002).
[6] H. Ohno, Science 281 (1998) 951.
[7] Y. Matsumoto, M. Murakami, T. Shono, T. Hasegawa, T. Fukumura, M. Kawasaki, P. Ahmet, T. Chikyow, S-Y. Koshihara, H. Koinuma, Science 291 (2001) 854.
[8] J. L. Costa-Kramer, F. Briones, J. F. Fernandez, A. C. Caballero, M. Villegas, M. Diaz, M. A. Garcia, A. Hernando, *"Nanotechnology"*,16 (2005) 214.
[9] D. C. Kundaliya, S. B. Ogale, S. E. Lofland, S. Dahr, C. J. Metting, S. R. Shinde, Z. Ma, B. Varughese, K. V. Ramanujachary, L. Salamanca-Riba, T. Venkatesan, *"Nature Materials",* 3 (2004) 709.
[10] R. C. Budhani, Prita Pant, R. K. Rakshit, K. Senapati, S. Mandal, N. K. Pandey, Jitendra Kumar, J. Phys., *"Condens. Matter"* 17 (2005) 75.
[11] H. Saeki, H. Matsui, T. Kawai, H. Tabata, J. Phys., *"Condens. Matter",* 16 (2004) S5533.
[12] S. B. Ogale, et al., *"Phys. Rev. Lett. 91"*, (2003) pp. 1-4.
[13] Zhenguo Ji, Zhenjie He, Yongliang Song, Kun Liu, Yin Xiang, *"Thin Solid Films",* 460 (2004) pp. 324–326.
[14] Matthias Batzill, James M. Burst, Ulrike Diebold, *"Thin Solid Film",* 484 (2005) pp.132-139.
[15] G. Korotcenkov, A. Cornet, E. Rossinyol, J. Arbiol, V. Brinzari, Y. Blinov, *"Thin Solid Films"* 471, (2005) pp. 310-319.
[16] M. Batzill, U. Diebold, *"Progress in Surface Science"*, 79 (2005) pp. 47–154.
[17] Pramod S. Patil, *"Materials Chemistry and Physics"*, 59 (1999) pp. 185-198.
[18] G. Korotcenkov, V. Macsanov, V. Brinzari, V. Tolstoy, J. Schwank, A. Cornet, J. Morante, *"Thin Solid Films"*, 467 (2004) pp. 209– 214.
[19]C. J. Huang, W. C. Shih, *"J. of Electronic Materials"*, vol. 32, No. 10 (2003).
[20] S. B. Ogale, et al., *"Phys. Rev. Lett."*, 91 (2003) pp. 1-4.
[21] T. Fukumura, H. Toyoaki, Y. Yamada, *"Semicond. Sci. Technol."*, 20 (2005) pp. 103-111.
[22] M. Batzill, Kh. Katsiev, J. M. Burst, U. *"Diebold, Phys. Rev. B"*, 72 (2005) 165414.
[23] M.-M. Bagheri-Mohagheghi, M. Shokooh-Saremi, *"Thin Solid Films"*, 441 (2003) pp. 238–242.
[24] A. Weibel, R. Bouchet, F. Boulch, P. Knauth, *"Chem. Mater."*, 17 (2005) pp. 2378-2385.
[25] L. J. Van der PAUW, *"Philips Technical Review"*, Vol. 20, No. 8 (1958/59) pp. 220-224.
[26] Z. A. Talib, Y. N. Loh, H. A. A. Sidek, W. M. D. W. Yusoff, W. M. M. Yunus, A. H. Shaari, *"Ceramics International"*, 30 (2004) 1715-1717.
[27] F. Yakuphanoglu, M. Arslan, *"Optical Materials"*, 27 (2004) pp. 29-37.
[28] M. Beaudoin, A. J. G. Devries, S. R. Johnson, H. Laman, T. Tiedje, *"Appl. Phys. Lett."*, 70(26) (1997) pp. 3540-3542.
[29] Timothy J. Coutts, David L. Young, Xiaonan Li, *"MRS Bulletin"*, August (2000) pp. 58-65.
[30] G. Korotcenkov, A. Cornet, E. Rossinyol, J. Arbiol, V. Brinzari, Y. Blinov, *"Thin Solid Films"*, 471 (2005) pp. 310-319.
[31] S. Venkataprasad Bhat, F. L. Deepak, *"Solid State Communications"*, 135 (2005) pp. 345-347.
[32] K. Gopinadhan, Dinesh K. Pandya, Subhash C. Kashyap, sujeet chaudhary, *"J. of Appl. Phys."*,. 99 (2006) 126106.
[33] J.Fayat, M. S. Castro, *"Journal of the European Ceramic Society"*, 23 (2003) 1585-1591.
[34] Tadatsugu Minami, *"MRS Bulletin"*, August (2000).
[35] Y. S. Feng, R. Sh. Yao, L. D. Zhang, Chin., *"Phy. Lett. 21"*, (2004) 1374.

مجله بلورشناسی و کانی‌شناسی ایران

سال شانزدهم، شمارهٔ ۴، زمستان ۸۷، از صفحهٔ ۶۶۴ تا ۶۷۵

اثر بازپخت در محیط آرگون و نیتروژن بر خواص ساختاری، الکتریکی و اپتیکی لایه‌های رسانای شفاف SnO_2:Co تهیه شده به روش اسپری پایرولیزیز

احمد قلی‌زاده، ناصر تجبر، محمد رضا علی‌نژاد

مشهد، دانشگاه فردوسی مشهد، گروه فیزیک، آزمایشگاه تحقیقاتی حالت جامد

Email: ah_gh1359@yahoo.com

(دریافت مقاله ۸۷/۱/۲۰ ، نسخه نهایی ۸۷/۹/۲۸)

چکیده: در این مقاله، لایه‌های نیمرسانای شفاف SnO_2 آلاییده با Co به روش اسپری پایرولیزیز تهیه شد و اثر گرمادهی در محیط آرگون و نیتروژن بر خواص ساختاری، الکتریکی و اپتیکی آن‌ها مورد بررسی قرار گرفت. لایه-های SnO_2:Co بر بستر شیشه در دمای ۴۸۰ °C با به‌کار بردن محلول آبی-اتانول شامل کلرید کبالت و کلرید قلع جایگذاری شد. مقدار ناخالصی کلرید کبالت از ۰ تا ۱۴ درصد وزنی در محلول تغییر داده شد. آنالیز طرح‌های پراش پرتو X نشان می‌دهد که پارامترهای a و V یاخته یکه چارگوشی با افزایش محتوی ناخالصی کاهش می‌یابد، در حالی‌که پارامتر c دارای یک کمینه‌ای در تراکم ۸ درصد وزنی ناخالصی پذیرنده یا نسبت اتمی $\frac{[Co]}{[Sn]}$ معادل با ۲۰ درصد اتمی در محلول است. بازپخت در محیط آرگون و نیتروژن سبب افزایش مقاومت ویژه الکتریکی، انرژی گاف نواری و شفافیت لایه‌های آلاییده با کبالت می‌شود.

واژه‌های کلیدی: *اکسیدهای رسانای شفاف، نیمرساناهای رقیق مغناطیسی، اسپری پایرولیزیز.*